A Shot-Noise Model for Paper Fibres with Non-uniform Random Orientations

JAN-OLOF JOHANSSON

Laboratory of Mathematics, IDE, Halmstad University

OLA HÖSSJER

Department of Mathematics, Stockholm University

ABSTRACT. The surface properties of newsprint and other paper qualities are to a great extent determined by the properties of the cellulose fibres. An appropriate description of these fibres as they appear in the paper is therefore important and can be used for quality classification and process monitoring. We suggest a model that considers the fibre geometry and appearance. It is based on a two-dimensional shot-noise process. The model is fit by minimizing a weighted least squares distance between the model-based and estimated covariance functions and this provides estimates of the fibre size, intensity and the non-uniform distribution of the fibre orientation. The model is applied to simulated and real data.

Key words: covariance function, fibre process, newsprint, shot-noise, weighted non-linear estimation

1. Introduction

The microstructure of newsprint has considerable importance for the paper quality and a good characterization of this structure is necessary for process monitoring and quality control. Especially the geometric properties of the fibres have vital importance. Currently, several procedures exist for measuring the geometry of the cellulose fibres. Most of them are based on measurements of fibres extracted from the pulp thus leaving the alterations of the fibres, which occur during the manufacturing process, unnoticed.

The properties of paper are highly determined by length, intensity and orientation of the fibres. In order to assess paper quality it is important to estimate these parameters from data. Traditionally, fibre length and intensity have been estimated assuming a uniform fibre orientation, as in Kallmes & Corte (1960), Warren (1970) and Dodson (1971). Fibre orientation, on the other hand, has been estimated separately, regarding fibre length and fibre intensity as nuisance parameters.

Many models of the microstructure of paper are devoted to model its mechanical properties, especially the strength. See for example Miles (1964), where anisotropic thick lines is a model for fibrous structures of thin sheets of paper. A common model for the fibre network is the Boolean germ-grain process of Matheron (1972, 1975), where locations of fibres form a two-dimensional Poisson process and fibre regions (the grains) are mutually independent random objects, which also are independent of the locations. An alternative approach was introduced by Mecke & Stoyan (1980). Their fibre system is based on fibre length measures on Borel sets. The advantage of this approach is that individual fibres need not be modelled, whereas the germ-grain process is easier to simulate from. For both models, the union of all fibres Ξ is the random object of interest, and inference is based on this set. The length and intensity of fibres can be estimated by counting the number of intersections between randomly chosen lines and Ξ. The orientation of fibres can be estimated by comparing the number of intersection between Ξ and lines with different directions, see e.g. Molchanov & Stoyan (1994) and Kärkkäinen *et al.* (2001). In the latter paper,

varying thickness of the fibres due to degraded imaging is taken into account. Line intersect counts are replaced by the local behaviour of scaled variograms, and then a weighted least squares objective function is used to estimate orientation parameters.

In this paper, we focus on properties that are important for the printing like surface roughness and the intention is to model thickness measurements of newsprint. The local thickness of newsprint depends not only on the properties of the fibres and other additives but also on the paper-making procedure. During manufacturing of newsprint, the cellulose fibres are distributed randomly into layers. Due to the intensity of fibres, their geometric properties and orientation, the local thickness of the final paper varies determined by the positions of the fibres. We model varying paper thickness by means of a two-dimensional shot-noise process (Daley, 1975; Westcott, 1976) and it includes fibre geometry, intensity and distribution of fibre orientation.

The model has been applied in a project involving Halmstad University and four Swedish paper mills. The main purpose of this project is to find the correlation between the surface properties of newsprint and the printing quality. As a part of the project we have developed the model to be used for characterizing the surface of the newsprint in terms of fibre parameters. A $2 \times 2 \ mm^2$ area of newsprint has been sampled and the local heights at 501×501 sample points comprise the data set used for the modelling. Figure 1 shows the two-dimensional observations viewed as an image, where the intensities correspond to the values of the local heights.

A model that comprises the fibre geometry, intensity and the non-uniform distribution of fibre orientation makes it possible to relate fibre mixtures to surface properties. As the fibre mixtures can be manipulated by the manufacturer, the model enables monitoring of the manufacturing process.

As cellulose fibres are approximately piecewise linear, a single fibre can be detected as several 'apparent rectangular fibres' with different orientation. For this reason, the marks of the shot-noise process consist of rectangles with varying orientation. In order to obtain a simple model with parameters of high informativeness, we make the simplifying assumption that all apparent fibres have the same length and width, so that in practice these parameters can be interpreted as mean length and mean width of fibres. The non-uniform orientation of the fibres is modelled through a von Mises distribution.

Our inference procedure is based on fitting observed mean and autocorrelations of height measurements, i.e. the local thickness, to those obtained from the shot-noise model by means of a weighted non-linear least squares procedure. In this way, we are able to estimate fibre intensity, width, length, thickness and the non-uniform distribution of fibre orientation simultaneously.
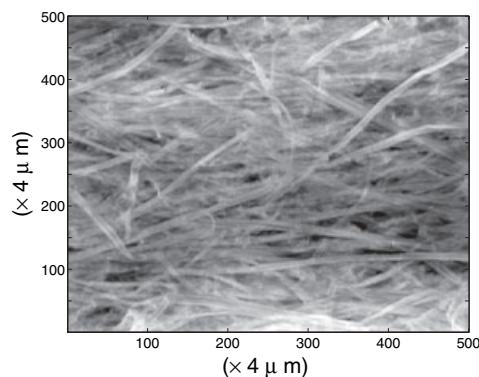

Fig. 1. Images of local heights on the surface of newsprint viewed as grey scale intensities.

The use of shot-noise processes in paper applications is not new. For instance, Deng & Dodson (1994) and Brown *et al.* (2003) consider a shot-noise process with circular objects as a way of modelling flocculation in paper. Brown *et al.* (2003) define an approximate ML-estimator based on Fourier transformed data along one manufacturing orientation when white noise is added to the shot-noise process.

This paper is organized as follows: The shot-noise process model is defined in section 2 and the matched autocorrelation estimator (MAE) in section 3. A simulation study is carried through in section 4, where the choice of starting value of the iterative estimation procedure is discussed in some detail. A real data example is analysed in section 5, whereas some further extensions of our method are proposed in section 6.

2. The shot-noise model

Consider a stochastic process $X(\mathbf{s})$, $\mathbf{s} \in \mathbb{R}^2$ of the form

$$X(\mathbf{s}) = \sum_i \Psi(\mathbf{s} - \mathbf{T}_i, \mathbf{U}_i), \ \mathbf{s} \in \Omega, \tag{1}$$

where $\{(\mathbf{T}_i, \mathbf{U}_i)\}$ is a stationary, independently marked point process on $\mathbb{R}^2$ with some mark space $\mathcal{U}$ and $\Psi : \mathbb{R}^2 \times \mathcal{U} \to R$ is a measurable non-negative function and Ω a subset of $\mathbb{R}^2$ where X is observed. We regard $\mathbf{T}_i$ as the position and $\mathbf{U}_i$ a vector specifying the size and orientation of the *i*th object. We further assume that $\{\mathbf{T}_i\}$ is a stationary Poisson point process on $\mathbb{R}^2$ with intensity λ. Models of the kind (1) have been studied by Matérn (1960), Barlett (1964) and in the shot-noise literature.

For simplicity, we assume that the objects are uniformly bounded in $\mathbb{R}^2$, i.e.

$$D = \bigcup_{\mathbf{u} \in \mathcal{U}} \{\mathbf{t}; \Psi(\mathbf{t}, \mathbf{u}) > 0\} \tag{2}$$

is a bounded subset of $\mathbb{R}^2$. Then, the mean $m_X = E(X(\mathbf{s}))$ and the covariance function $r_{X(\tau)} = \mathrm{Cov}(X(\mathbf{s}), X(\mathbf{s} + \tau))$ are given by

$$m_X = \lambda \int E(\Psi(\mathbf{t}, \mathbf{U})) \mathrm{d}\mathbf{t}, \tag{3}$$

and

$$r_X(\tau) = \lambda \int E(\Psi(\mathbf{t}, \mathbf{U}) \cdot \Psi(\mathbf{t} + \tau, \mathbf{U})) \mathrm{d}\mathbf{t} \tag{4}$$

respectively, provided that the integrals are finite, see Johansson & Hössjer (2001). Because of (2), this is the case if Ψ attains only the values 0 and $c > 0$. With

$$A_{\mathbf{u}} = \{\mathbf{t} : \Psi(\mathbf{t}, \mathbf{u}) = c\} \tag{5}$$

we get

$$m_X = c\lambda E|A_{\mathbf{U}}| \tag{6}$$

and

$$r_X(\tau) = c^2 \lambda E(|A_{\mathbf{U}} \cap (A_{\mathbf{U}} + \tau)|). \tag{7}$$

Here, $|A|$ is the Lebesque measure of the two-dimensional set A and $A + \tau$ denotes translation of A by the vector τ.

To model newsprint cellulose fibres, we consider rectangular objects, with $\mathbf{u} = (l, w, v)$,

$$\psi(\mathbf{t}, \mathbf{u}) = c \cdot 1_{\{|\mathbf{t} \cdot \mathbf{e}_v| \leq l/2; |\mathbf{t} \cdot \mathbf{e}_v^\perp| \leq w/2\}}, \tag{8}$$

$\mathbf{e}_v = (\cos(v), \sin(v))$ and $\mathbf{e}_v^\perp = (\sin(v), -\cos(v))$. Here $l > 0$ and $w > 0$ are the length and width of the rectangle and $v \in (-\pi/2, \pi/2]$ is the orientation. The fibre preferred orientation is denoted v_0.

We assume the random object $\mathbf{U}$ has independent components L, W and V. The angle distribution of V can conveniently be modelled from the von Mises family of distributions, cf. Mardia & Jupp (2000). Then the density of V is given by

$$f_V(v) = \frac{1}{k(\sigma)} \exp((1/\sigma - 1)\cos^2(v - v_0)), \quad -\pi/2 < v \leq \pi/2, \tag{9}$$

where

$$k(\sigma) = \int_{-\pi/2}^{\pi/2} \exp((1/\sigma - 1)\cos^2(v - v_0)) \mathrm{d}v \tag{10}$$

is a normalizing constant. The parameter $\sigma \in [0, 1]$ is a measure of dispersion and indicates how concentrated the distribution is around v_0. For $\sigma = 1$, the distribution is uniform and for $\sigma = 0$, it is a one-point distribution, where the probability of the orientation v_0 is 1. Figure 2 shows the density functions for three different values of σ.

The mean and the covariance function of the process can now be expressed with the following proposition.

Proposition 1
Let $\mathbf{X}$ *be a shot-noise process with rectangular shot effects in* $\mathbb{R}^2$ *with length* L, *width* W, *orientation* V *and covariance vector* $\boldsymbol{\tau} = \|\boldsymbol{\tau}\|(\cos\theta, \sin\theta)$, *for* $\theta \in (-\pi/2, \pi/2]$.
   Then,

$$m_{\mathbf{X}} = c\lambda E[L]E[W] \tag{11}$$

and

$$r_X(\boldsymbol{\tau}) = c^2 \lambda E[(L - \|\boldsymbol{\tau}\| |\cos(V - \theta)|)_+ (W - \|\boldsymbol{\tau}\| |\sin(V - \theta)|)_+] \tag{12}$$

$$= c^2 \lambda \int_{-\pi/2}^{\pi/2} E[(L - \|\boldsymbol{\tau}\| |\cos(v - \theta)|)_+] \cdot$$

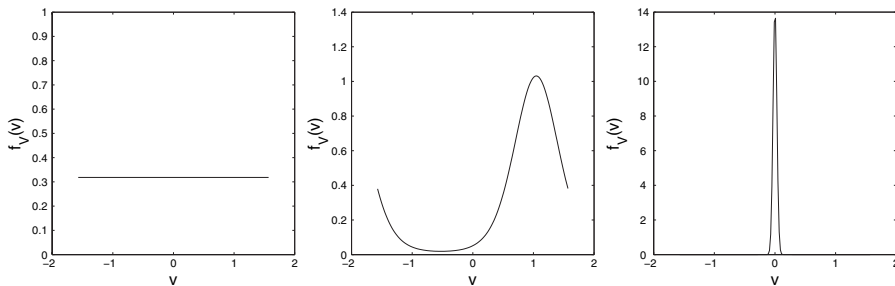$$E[(W - \|\boldsymbol{\tau}\| |\sin(v - \theta)|)_+] f_V(v) \mathrm{d}v.$$

Fig. 2. Graphs of the angle densities for $\sigma = 1$ (left), $\sigma = 0.2$ (middle) and $\sigma = 0.002$ (right). Note that for $\sigma = 1$, the distribution is uniform and when $\sigma \to 0$, the distribution tends to a one-point distribution. The figure in the middle illustrates the periodic nature of the density. In this figure $v_0 = \pi/3$.
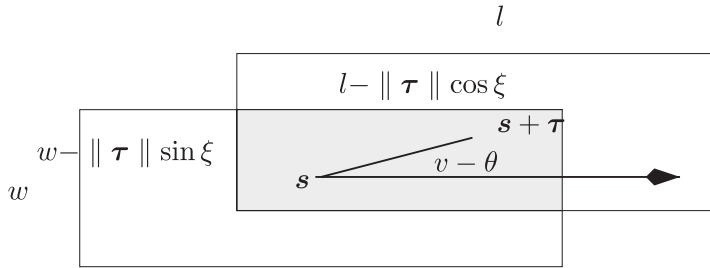
Fig. 3. The shaded area within the centre of a rectangle with sides w and l will cover both $\mathbf{s}$ and $\mathbf{s} + \tau$.

Proof. From (5) and (8), we have $A_{\mathbf{u}} = \{\mathbf{t}; 1_{\{\|\mathbf{t} \cdot \mathbf{v}\| \le l/2 \cdot \|\mathbf{t} \cdot \mathbf{v}^\perp\| \le w/2\}}\}$, which gives the area of $A_{\mathbf{u}} = lw$ and then, according to (6), the mean $m_{\mathbf{X}} = c\lambda E[L]E[W]$.

From (7) we get the covariance function by computing the area $A_{\mathbf{u}} \cap A_{\mathbf{u}} + \tau$. For given length, width, orientation and covariance vector τ, this rectangular area equals the area of the intersection of two rectangles with the same orientation and with centres in $\mathbf{s}$ and $\mathbf{s} + \tau$. This area is found by calculating the projections of the covariance vector τ along the orientation of the length, which is $\|\tau\| |\cos(v - \theta)|$ and perpendicular to this orientation, which is $\|\tau\| |\sin(v - \theta)|$. The sides of the rectangle are thus $(l - \|\tau\| |\cos(v - \theta)|)_+$ and $(w - \|\tau\| |\sin(v - \theta)|)_+$ and the area of $A_{\mathbf{u}} \cap A_{\mathbf{u}} + \tau = (w - \|\tau\| |\sin(v - \theta)|)_+ (l - \|\tau\| |\cos(v - \theta)|)_+$; cf. Figure 3.

When the fibres have constant length and width, (10) and (11) simplify to

$$m_{\mathbf{X}} = c\lambda lw \tag{13}$$

and

$$r_{\mathbf{X}}(\tau) = c^2 \lambda \int_{-\pi/2}^{\pi/2} (l - \|\tau\| |\cos(v - \theta)|)_+ \cdot (w - \|\tau\| |\sin(v - \theta)|)_+ \cdot f_V(v)\mathrm{d}v, \tag{14}$$

with f_V defined as in (9). This integral has no explicit expression but can be solved numerically.

Remark. As a special case we consider the situation with fixed lengths and widths but with the orientation angle, V uniformly distributed, $V \in \text{Rect}(-\pi/2, \pi/2]$, i.e. for $\sigma = 1$ in (9). This case was described in Dodson (1971). By (14) we obtain,

$$r_{\mathbf{X}}(\tau) = \frac{c^2 \lambda}{\pi} \int_{-\pi/2}^{\pi/2} (l - \|\tau\| |\cos(v - \theta)|)_+ (w - \|\tau\| |\sin(v - \theta)|)_+ \mathrm{d}v \tag{15}$$

$$= \begin{cases} c^2 \lambda wl \left(1 - \frac{2}{\pi}\left(\frac{\|\tau\|}{l} + \frac{\|\tau\|}{w} - \frac{\|\tau\|^2}{2lw}\right)\right) & \text{for } 0 < \|\tau\| \le w, \\ \frac{2c^2 \lambda wl}{\pi}\left(\arcsin\left(\frac{w}{\|\tau\|}\right) - \frac{w}{2l} - \frac{\|\tau\|}{w} + \sqrt{\frac{\|\tau\|^2}{w^2} - 1}\right) & \text{for } w < \|\tau\| \le l, \\ \frac{2c^2 \lambda wl}{\pi}\left(\arcsin\left(\frac{w}{\|\tau\|}\right) - \arccos\left(\frac{l}{\|\tau\|}\right) \right. \\ \qquad \left. - \frac{w}{2l} - \frac{l}{2w} - \frac{\|\tau\|^2}{2lw} + \sqrt{\frac{\|\tau\|^2}{l^2} - 1}\right) & \text{for } l < \|\tau\| \le \sqrt{l^2 + w^2}. \end{cases}$$

3. Estimation of model parameters

From realizations of the process, we can estimate $m_{\mathbf{X}}$ and $r_{\mathbf{X}}(\tau)$. These moments depend on the parameters of the process. In our model, these include the height parameter, c, the intensity, λ,

the parameters of the distribution of the length, the width and the fibre orientation. In this paper, we only consider a simplified model and assume that the unknown lengths and widths, l and w, are of equal size for all fibres. It would be possible to allow L and W to be stochastic with one location and one dispersion parameter for each. However, we believe the estimation problem then becomes more ill-conditioned. Instead, we interpret l and w as location parameters for the true underlying distributions of L and W. The angle is assumed to have a distribution according to (9), which is fully characterized by the parameters σ and v_0.

We assume that v_0 is known and thus summarize the parameters of the process in a parameter vector,

$$\xi = (c, \lambda, l, w, \sigma). \tag{16}$$

The mean function, $m_{\mathbf{X}}$ and the covariance function, $r_{\mathbf{X}}(\tau)$ can now be expressed as functions of ξ.

In the paper application, the process $\mathbf{X}$ can only be observed at discrete points and we introduce a lattice,

$$\Gamma = \{\mathbf{s}_1, \mathbf{s}_2, \ldots, \mathbf{s}_M\}, \ \ \mathbf{s}_i \in \Omega; \ i = 1, \ldots, M, \tag{17}$$

as a finite number of points in Ω.

The estimation of the fibre geometry assumes that realizations are studied in an area large enough to eliminate the effects of the borders. This implies some knowledge of the fibre length and width, properties that we are to estimate. We base the size of this area on measurements from other investigations.

For the estimation we now get the system of equations:

$$\begin{cases} r_{\mathbf{X}}(\mathbf{0})/m_{\mathbf{X}} & = c \\ m_{\mathbf{X}}^2/r_{\mathbf{X}}(\mathbf{0}) & = \lambda l w \\ r_{\mathbf{X}}(\tau)/r_{\mathbf{X}}(\mathbf{0}) & = E\left[\left(1 - \frac{\|\tau\|}{l}|\cos(V - \theta)|\right)_+ \cdot \left(1 - \frac{\|\tau\|}{w}|\sin(V - \theta)|\right)_+\right] \\ & =: f_\tau(l, w, \sigma), \end{cases} \tag{18}$$

where the expectation in (18) is taken with respect to V according to the distribution in (9). Recalling that we observe $\mathbf{X}$ on the grid Γ in (17), we can estimate the quantities of the LHS of (18) by means of

$$\hat{m}_{\mathbf{X}} = \frac{1}{M} \sum_{s \in \Gamma} \mathbf{X}(\mathbf{s}) \tag{19}$$

and

$$\hat{r}_{\mathbf{X}}(\tau_i) = \frac{1}{M} \sum_{\substack{\mathbf{s} \in \Gamma \\ \mathbf{s}+\tau_i \in \Gamma}} (\mathbf{X}(\mathbf{s}) - \hat{m}_{\mathbf{X}})(\mathbf{X}(\mathbf{s} + \tau_i) - \hat{m}_{\mathbf{X}}), \quad i = 1, \ldots, K, \tag{20}$$

where each τ_i can be written as $\mathbf{s}_k - \mathbf{s}_j$ for some $\mathbf{s}_j, \mathbf{s}_k \in \Gamma$. Viewing $\hat{r}_{\mathbf{X}}(\tau_i)/\hat{r}_{\mathbf{X}}(\mathbf{0})$ as a noisy observation of $f_{\tau_i}(l, w, \sigma)$, we can use weighted non-linear least squares, cf. Draper & Smith (1998), to estimate (l, w, σ) according to

$$\begin{cases} (\hat{l}, \hat{w}, \hat{\sigma}) & = \arg\min_{(l,w,\sigma)} \sum_{i=1}^{K} v_i \left(\frac{\hat{r}(\tau_i)}{\hat{r}(\mathbf{0})} - f_{\tau_i}(l, w, \sigma)\right)^2 \\ \hat{c} & = \hat{r}_{\mathbf{X}}(\mathbf{0})/\hat{m}_{\mathbf{X}} \\ \hat{\lambda} & = \hat{m}_{\mathbf{X}}^2/(\hat{r}_{\mathbf{X}}(\mathbf{0})\hat{l}\hat{w}), \end{cases} \tag{21}$$

where $\{v_i\}_{i=1}^{K}$ is a preselected set of weights.

We refer to the estimator (21) of ξ as the matched autocorrelation estimator, (MAE), cf. Rue & Tjelmeland (2002), even though it is only three of the parameters, l, w and σ, that are estimated by fitting the autocorrelation function.

4. A simulation study

In this section, we perform a simulation study of the MAE (24). By using simulated fibre processes with known parameter values, we obtain estimates of a variety of parameter combinations, which we compare with the specified values of the parameters. The simulated processes are observed on a quadratic grid, Γ, of size 512×512 points with grid distance equal to 1. Figure 4 shows an example of such a simulated process.

In total, 32 different parameter combinations have been investigated. For four values of the angle parameter, we have chosen two values of the length, two values of the width and two values of the intensity, $\lambda = 0.0025$ and $\lambda = 0.005$. Each parameter combination includes 100 simulated replicates thus making it possible to compute the standard errors.

For simplicity of implementation, we have chosen weights v_i in (21) equal to 1 when τ_i lies along the fibre preferred orientation v_0 or its orthogonal orientation $v_0 + \pi/2$ and equal to 0 otherwise. We believe the information loss with this choice of weights is small compared to including more terms in (21) for lags τ_i in other orientations.

4.1. Implementation issues for the matched autocorrelation estimator

We assumed in section 3 that the fibre preferred orientation v_0 was known. For instance, we may have prior knowledge of v_0. Alternatively, v_0 can be estimated using the estimated covariance function in (21) or using image analysis methods, where the property that the contours have maximal distance from the origin along the fibre preferred orientation can be utilized.

4.1.1 Starting values for the length and the width

The estimated covariance function in the fibre preferred orientation and the orthogonal orientation can be used to determine starting values for the length, l and the width, w.

With v_0 known, we may without loss of generality put $v_0 = 0$. Starting out from Equation (18) with $\theta = 0$ and $\rho = \|\tau\|$ we then get
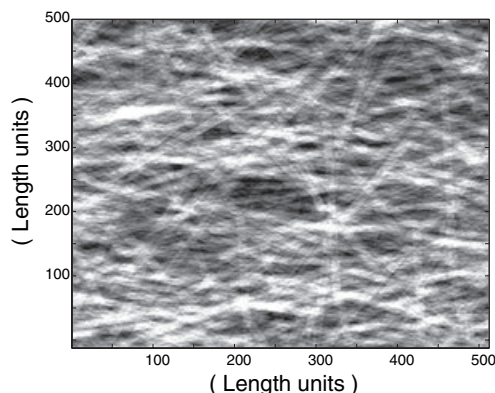

Fig. 4. An illustration of a simulation of the newsprint fibrous network. The parameter values are $\lambda = 0.0025$, $l = 300$, $w = 15$ and $\sigma = 0.2$.

$$r_{\mathbf{X}}(\rho, 0) = \frac{c^2 \lambda}{k(\sigma)} \int_{-\pi/2}^{\pi/2} (l - \rho|\cos(v)|)_+ \cdot (w - \rho|\sin(v)|)_+ f_V(v) \mathrm{d}v \tag{22}$$

and

$$r_{\mathbf{X}}(\rho, \pi/2) = \frac{c^2 \lambda}{k(\sigma)} \int_{-\pi/2}^{\pi/2} (l - \rho|\sin(v)|)_+ \cdot (w - \rho|\cos(v)|)_+ f_V(v) \mathrm{d}v. \tag{23}$$

For $\sigma = 0$, these equations become

$$r_{\mathbf{X}}(\rho, 0) = c^2 \lambda (l - \rho)_+ w \tag{24}$$

in the fibre preferred orientation and

$$r_{\mathbf{X}}(\rho, \pi/2) = c^2 \lambda (w - \rho)_+ l, \tag{25}$$

in the orthogonal direction. As can be seen from these equations, the covariance function equals zero when $\rho > l$ in the fibre preferred orientation and for $\rho > w$ in the orthogonal orientation. Also when the parameter σ in the angle distribution differs from 0, there is a breakpoint in the covariance functions, which easily can be detected in the graphs, cf. Fig. 5.

4.1.2 Starting values for the parameter σ in the distribution of the fibre orientation

As a starting value of the parameter σ, we have utilized the local scaling of the variogram around the origin. If $\tau = \rho(\cos \theta, \sin \theta)$ and

$$\begin{aligned} \rho_{\mathbf{X}} &= 2(r_{\mathbf{X}}(0) - r_{\mathbf{X}}(\tau)) \\ &= 2\beta(\theta)\rho^\alpha + o(\rho^\alpha) \end{aligned} \tag{26}$$

as $\rho \searrow 0$ and θ is kept fixed, we refer to $\beta(\theta)$ as the topothesy in the direction θ and α as the fractal index, cf. Davies & Hall (1999). For the fibre process it turns out that $\alpha = 1$, whereas

$$F(\sigma) := \frac{\beta(v_0) + \beta(v_0 + \pi/2)}{\int_{v_0}^{v_0+\pi/2} \beta(\theta) \mathrm{d}\theta} \tag{27}$$

only depends on σ, cf. Johansson & Hössjer (2001) for calculations of $\beta(\theta)$ and $F(\sigma)$. Now $\beta(\theta)$ can be estimated from data by applying ordinary least squares estimation based on the logarithm of the variogram, since
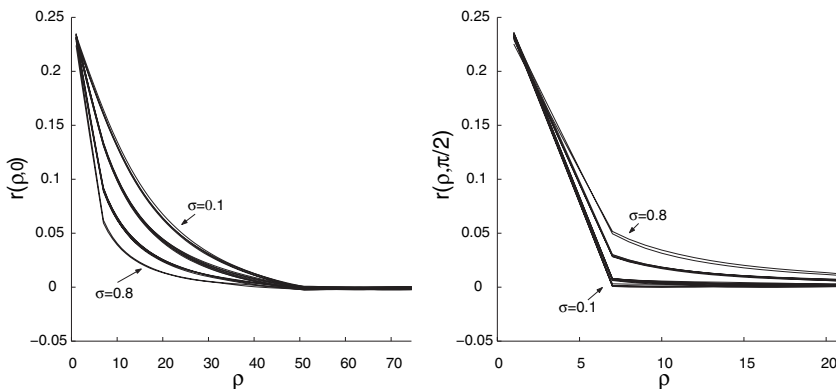

Fig. 5. The left figure shows the graphs of the estimated covariance function in the fibre preferred orientation, $r(\rho, 0)$ and the right figure in the orthogonal orientation, $r(\rho, \pi/2)$. The fibre length equals 50 units, the width equals 6 units and the angle parameter σ equals 0.1, 0.2, 0.4 and 0.8, respectively.

$$\log \rho_{\mathbf{X}}(\boldsymbol{\tau}) = \log \beta(\theta) + \alpha \log \rho + o(\log \rho), \tag{28}$$

cf. Constantine & Hall (1994). By plugging in the estimates of $\beta(\theta)$ for several directions into (27), we get an estimate, $\hat{F}$, of $F(\sigma)$. When the parameter σ varies from 0 to 1, the distribution of direction angles varies from a one-point distribution to a uniform distribution and the function $F(\sigma)$ from 1 to $4/\pi$, see Fig. 6. $F(\sigma)$ is monotonically increasing in [0, 1] and we find the intersection of $F(\sigma)$ with the line $y = \hat{F}$ by successively testing the midpoints of sub-intervals.

4.1.3 Summary
We sum up the implementation of the MAE in the following steps.

- The preferred orientation normally equals the orientation of manufacture, which means that v_0 is assumed to be equal to zero. Is this is in doubt, v_0 is estimated by using the two-dimensional covariance function and image analysis methods.
- Starting values for the length and the width are based on the covariance functions in the orientation v_0 and $v_0 + \pi/2$. The values are estimated by using standard image analysis methods for finding the breakpoints described in section 4.1.1 and illustrated in Fig. 5.
- Starting values for the orientation parameter σ are determined as described in section 4.1.2.
- Estimates of the three parameters (l, w, σ) are computed iteratively from the autocorrelation function according to (21), using weighted non-linear least squares, with starting parameters as determined from the previous steps.
- Estimates of c and λ are computed from (24), using the estimated values of (l, w, σ) from the previous step as plug-in.

A simulation study with different starting values has also been performed. Since the starting values are chosen according to the observed breakpoints of the graphs, they may be difficult to determine precisely. However, the simulation study shows that the values chosen in this way do not affect the parameter estimates.

4.2. Conclusions

The results from the simulation experiment with intensity equal to 0.005 are listed in Table 1. The other investigated intensity, 0.0025, shows similar results and are not presented here.
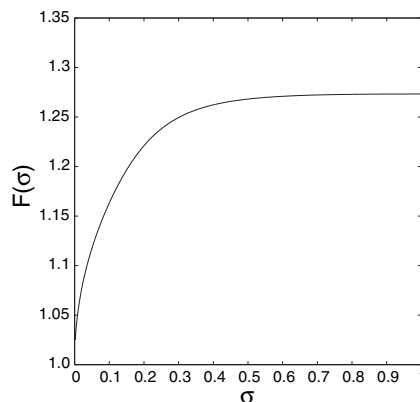

Fig. 6. Graph of the function $F(\sigma)$.

Table 1. *Results from a simulation study with intensity $\lambda = 0.0050$ and $c = 1$. For each combination of parameter values, 100 replicates have been simulated*

Specified values			Estimated values								
			$\hat{l}$		$\hat{w}$		$\hat{\sigma}$		$\hat{\lambda} \times 10^4$		$\hat{c}$
l	w	σ	Mean	SE	Mean	SE	Mean	SE	Mean	SE	Mean	SE
50	6	0.1	51.48	2.23	6.35	0.04	0.12	0.01	49	0.2	1.01	0.005
50	6	0.2	51.21	1.42	5.96	0.03	0.23	0.01	38	0.3	1.01	0.006
50	6	0.4	47.38	1.98	5.47	0.01	0.35	0.00	53	0.1	1.01	0.005
50	6	0.8	49.76	3.18	5.36	0.04	0.87	0.00	48	0.3	1.02	0.007
50	3	0.1	49.51	3.84	3.18	0.10	0.11	0.02	52	0.4	1.01	0.005
50	3	0.2	53.57	1.88	3.08	0.03	0.24	0.01	49	0.3	1.01	0.005
50	3	0.4	49.86	3.27	2.77	0.01	0.40	0.01	47	0.4	1.01	0.004
50	3	0.8	79.48	9.99	2.69	0.01	0.82	0.04	46	0.4	1.01	0.005
25	6	0.1	24.69	0.39	6.10	0.04	0.11	0.01	51	0.2	1.00	0.004
25	6	0.2	25.32	0.71	5.72	0.04	0.22	0.01	48	0.3	1.01	0.005
25	6	0.4	25.45	0.71	5.45	0.05	0.41	0.01	52	0.3	1.01	0.003
25	6	0.8	26.70	1.75	5.47	0.01	0.77	0.03	49	0.4	1.01	0.004
25	3	0.1	24.37	0.19	3.02	0.04	0.10	0.00	48	0.3	1.01	0.006
25	3	0.2	26.13	0.78	2.84	0.03	0.22	0.00	49	0.4	1.01	0.005
25	3	0.4	25.48	1.35	2.73	0.01	0.41	0.01	49	0.3	1.01	0.007
25	3	0.8	30.21	0.92	2.66	0.00	0.80	0.01	48	0.5	1.01	0.007

SE, standard error.

The weighted non-linear least squares estimator of the covariance function performs reasonably well for a wide variety of parameter combinations. The scale and intensity parameters are those which give the best estimates with respect to bias and standard error. For some combinations of parameters, especially large fibre length and large σ-values, the procedure may diverge or oscillate between two different values and not give any estimates. Such behaviour of the non-linear regression technique is also described in the literature, cf. Draper & Smith (1998). We also note that for small w and large σ the estimates of the length are not very good. These results might depend on the small variation of the covariance function in the preferred orientation for values of $\|\tau\|$ close to the fibre length. Compare the flat shape of the corresponding graphs as shown in Fig. 5. Another problem is the estimates of w, which seem to be biased with increasing values of σ. However, for the paper application, this is not a serious disadvantage since the distribution of fibre orientation is concentrated around the preferred direction and the parameter σ is < 0.4 for most paper qualities.

5. Application

We have investigated the surface topography of a rectangular piece of newsprint of size 2×2 mm^2 made from soft-wood without any return fibres, cf. Fig. 1.

The measurements are performed using a stylus instrument, which samples the surface on a grid with 4 μm between the samples points, see Benett & Dancy (1981) for details on the measuring. In total, there are 501×501 sample points. The choice of such a small area may cause edge effects but the measurements can be performed during a reasonable short time which is desirable for industrial applications.

Figure 7 shows the estimated covariance functions in the fibre preferred orientation and the orthogonal orientation. The results of the estimation are listed in Table 2. Based on these
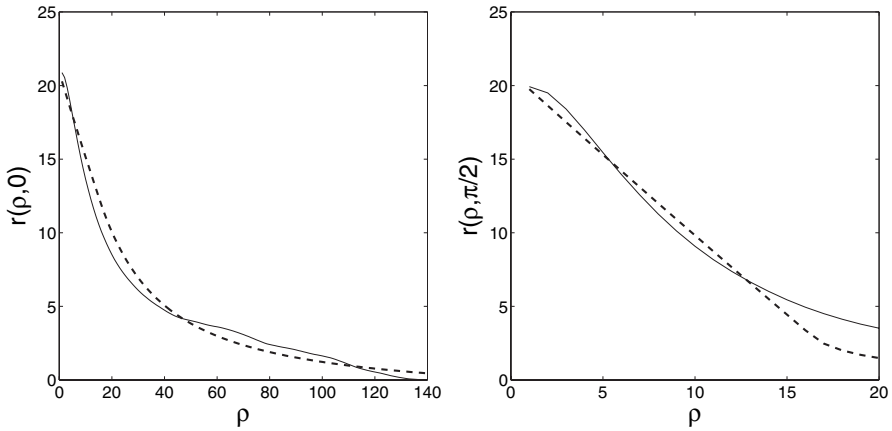
Fig. 7. Plots of the estimated covariance functions of the newsprint application $r(\rho, 0)$ (left) and $r(\rho, \pi/2)$ (right). The dashed lines are the model-based estimates and solid lines the non-parametric estimates.

Table 2. *Results of estimation of fibre geometry and fibre intensity on newsprint. The grid-size* 4 *μm is used as length unit. The starting values were* $l = 120$, $w = 12$ *and* $\sigma = 0.12$

| $\hat{l}$ | Estimated values (length units) | | | |
	$\hat{w}$	$\hat{\sigma}$	$\hat{\lambda}$	$\hat{c}$
375.2 (19.0)	12.17 (0.36)	0.27 (0.02)	0.0037 (0.004)	1.12 (0.05)
	Estimated values (mm)			
1.501 (0.076)	0.049 (0.002)	0.27 (0.02)	238 (25)	0.0045 (0.0002)

The values in parentheses are the standard errors.

estimates, we simulate realizations of the fibre process and for each such realization we estimate model parameters according to (21). The standard errors are then calculated from the bootstrapped parameter estimates.

As a validation of the model we compared $\hat{m}_X$ in (19) and $\hat{r}_X$ in (20) along the fibre preferred orientation and the orthogonal orientation with (13)–(14), using estimated values of Table 2 as plug-in. The two estimates of m_X were 18.92 (model-based) and 19.01 (non-parametric) and the two covariance functions are shown in Fig. 7 for each orientation. This indicates a good fit between the non-parametric and the model-based estimates of m_X and r_X.

The results in Table 2 correspond well to other results concerning fibre length and fibre widths; cf. Deng & Dodson (1994) and references therein. We have not found any model in the literature comprising fibre geometry, intensity and distribution of fibre orientation and it has therefore not been possible to make comparisons with other research. This paper may pioneer in estimation of all these properties within the same model.

6. Conclusions

We have proposed a general parametric model for fibre geometry, intensity and non-uniform distribution of fibre orientation and an estimator of these parameters. The model is tested in a newsprint application to study the surface roughness for a specified pulp mixture.

In our implementation, two-dimensional measurement are only needed for the computation of the starting value of σ. If therefore, some prior knowledge of the parameter σ is available, it

suffices to measure the paper in the fibre main and its orthogonal orientations. The method is thus easy to use in paper industry because standard measurements can be utilized.

A possible generalization of the model is to consider a superposition of two shot-noise processes, one fibre process with rectangular objects and one cluster process with larger circular objects. In this way both the fibre geometry and the fibre flocculation can be modelled, see Johansson & Hössjer (2001).

A further application is to use the vector ξ (or a subset of it) to cluster or discriminate between various paper types. For instance, if several samples of each type of paper are available, one could use a random effects model, with ξ having a separate distribution in $\mathbb{R}^5$ for each type of paper. See also Johansson (2002), where estimated values of the fractal index and topothesy are used for discrimination.

The proposed estimator of model parameters, the MAE, is based on fitting observed mean and autocorrelations. An alternative approximate ML procedure can be defined by noting that the vector $\mathbf{X} = (X(\mathbf{s}_1), \ldots, X(\mathbf{s}_M))$ is asymptotically normal as the intensity λ tends to infinity, cf. Papoulis (1971), Rice (1977) and Heinrich & Schmidt (1985). Hence, provided λ is reasonably large, we may approximate the distribution of $\mathbf{X}$ by $N(\mathbf{m}, \boldsymbol{\Sigma})$, where $\mathbf{m} = (m_{\mathbf{X}}, \ldots, m_{\mathbf{X}})$ and $\boldsymbol{\Sigma} = (r_{\mathbf{X}}(\mathbf{s}_i + \mathbf{s}_j))_{ij}$. This approach has computational disadvantages, however, since we need to invert the large matrix $\boldsymbol{\Sigma}$. Another faster and approximate ML-estimator can be defined in terms of the two-dimensional Fourier transform of X, see Brown *et al.* (2003) in the context of shot-noise processes with circular objects. It would be interesting to compare the performance of the MAE with this estimator.

Acknowledgments

References

Barlett, M. S. (1964). The spectral analysis of two-dimensional point processes. *Biometrika* **51**, 299–311.

Benett, J. & Dancy, J. (1981). Stylus profiling instrument for measuring statistical properties of smooth optical surfaces. *Appl. Opt.* **20**, 1785–1802.

Brown, P., Diggle, P. & Henderson, R. (2003). A non-Gaussian spatial process model for opacity of flocculated paper. *Scand. J. Statist.* **30**, 355–368.

Constantine, A. & Hall, P. (1994). Characterizing surface smoothness via estimation of effective fractal dimension. *J. Roy. Statist. Soc. Ser. B* **56**, 97–113.

Daley, D. (1975). The definition of a multi-dimensional generalization of shot noise. *Appl. Probab.* **8**, 128–135.

Davies, S. & Hall, P. (1999). Fractal analyses of surface roughness by using spatial data. *J. Roy. Statist. Soc. Ser. B* **61**, 3–37.

Deng, M. & Dodson, C. (1994). *Paper. An engineered stochastic structure*. Tappi Press, Atlanta.

Dodson, C. (1971). Spatial variability and the theory of sampling in a random fibrous network. *J. Roy. Statist. Soc. Ser. II B* **33**, 88–94.

Draper, N. & Smith, H. (1998). *Applied regression analysis*, 3rd edn. John Wiley & Sons, New York.

Heinrich, L. & Schmidt, V. (1985). Normal convergence of multidimensional shot noise and rates of this convergence. *Adv. Appl. Probab.* **17**, 709–730.

Johansson, J.-O. (2002). *Models of surface roughness with applications in paper industry*. PhD Thesis, Lund Institute of Technology, Lund.

Johansson, J.-O. & Hössjer, O. (2001). *Parametric models and estimators of fiber and cluster processes*. Preprint 2001:30, Lund Institute of Technology, Lund.

Kallmes, O. & Corte, H. (1960). The structure of paper, I. The statistical geometry of an ideal two dimensional fibre network. *Tech. Assoc. Pulp Paper. Ind.* **44**, 519–528.

Kärkkäinen, S., Penttinen, A., Ushakov, N. & Ushakova, A. (2001). Estimation of orientation characteristic of fibrous material. *Adv. in Appl. Prob.* **33**, 559–575.

Mardia K. & Jupp, P. (2000). *Directional statistics.* John Wiley & Sons, Chichester.

Matérn, B. (1960). Spatial variation. *Meddelande från Statens Skogsforskningsinstitut* **49**, 1–144.

Matheron, G. (1972). Ensamles fermés aléatoires ensambles semi-Markov et polyèdres poissoniens. *Adv. Appl. Probab.* **4**, 508–541.

Matheron, G. (1975). *Random sets and integral geometry.* John Wiley & Sons, New York.

Mecke, J. & Stoyan, D. (1980). Formulas for stationary planar fibre processes I – general theory. *Math. Operationsforsch. Statist. Ser. Statist.* **11**, 267–279.

Miles, R. (1964). Random polygons determined by random lines in a plane. *Proc. Natl. Acad. Sci. USA* **52**, I 901–907, II 1157–1160.

Molchanov, I. & Stoyan, D. (1994). Directional analysis of fibre processes related to Boolean model. *Metrica* **41**, 183–199.

Papoulis, A. (1971). High density shot noise and Gaussianity. *J. Appl. Probab.* **8**, 118–127.

Rice, J. (1977). On generalized shot noise. *Adv. Appl. Probab.* **9**, 553–565.

Rue, H. & Tjelmeland, H. (2002). Fitting Gaussian Markov Random Fields to Gaussian Fields. *Scand. J. Statist.* **29**, 31–49.

Warren, W. (1970). Estimates of fiber length a detailed formulation. *Tappi J.* **53**, 1494–1499.

Westcott, M. (1976). On the existence of a generalized shot noise process. In *Studies in probability and statistics* (ed. E. Williams). North-Holland, Amsterdam, 73–88.

Jan-Olof Johansson, Laboratory of Mathematics, IDE, Halmstad University, Box 823, S-301 18 Halmstad, Sweden.
E-mail: jan_olof.johansson@ide.hh.se